Thermoporometry as a new tool in analyzing mesoporous MCM-41 materials

K.R. Kloetstra [a,1], H.W. Zandbergen [b], M.A. van Koten [a] and H. van Bekkum [a]

[a] *Laboratory for Organic Chemistry and Catalysis, Delft University of Technology, Julianalaan 136, 2628 BL Delft, The Netherlands*

[b] *Laboratory for Materials Science, Delft University of Technology, Rotterdamseweg 137, 2628 AL Delft, The Netherlands*

Received 26 September 1994; accepted 19 April 1995

Thermoporometry, a calorimetric procedure, is applied for measuring the pore size distribution, pore volume and surface area of mesoporous MCM-41 molecular sieves using water as the adsorbate. A series of MCM-41 materials with various pore diameters was synthesized and subjected to the new method. The results are compared with nitrogen physisorption. Both methods are complementary, whereby the former provides also information about the pore shape. MCM-41 materials with pores wider than 50 Å also allow the use of benzene as the adsorbate in thermoporometry.

Keywords: thermoporometry; pore size; pore shape; MCM-41

1. Introduction

The sorption of gases is a widely used standard technique for characterization of mesoporous solids. Thus, by measuring the adsorption isotherm of nitrogen at low temperature, the specific surface area, pore volume and pore size distribution are calculated [1–3]. During the adsorption process, nitrogen condenses in the pores to form a metastable liquid phase in a process known as capillary condensation. The condensation pressure is an increasing function of the pore size. It is given by the Kelvin equation.

Physisorption of nitrogen and cyclopentane onto MCM-41 material, a member of the mesoporous M41S molecular sieve family [4,5], with pore sizes smaller than 43 Å showed isotherms of the unusual reversible type IV [6–10]. On the other hand, MCM-41 with an average pore diameter of 45 Å showed hysteresis [9,10]. For the adsorption of argon and oxygen, a significant hysteresis has been observed [7–9]. Some authors ascribe this to a transition from "secondary micropores" to mesopores [9]. Freezing phenomena in water-saturated MCM-41 systems with var-

[1] To whom correspondence should be addressed.

ious pore dimensions were studied with ^{1}H NMR spectroscopy [10,11]. For MCM-41 materials with pore sizes smaller than 40 Å no hysteresis was found.

In this paper, we report on the use of thermoporometry for analyzing mesoporous molecular sieves. Thermoporometry [12] is based on the fact that conditions of the equilibrium of the solid, liquid and gaseous phases of a pure substance depend on the curvature of the solid–liquid interphase. In the case of a liquid contained in a porous material the solid–liquid interphase curvature is closely related to the dimensions of the pore. By recording a solidification thermogram of a pure condensate inside a porous material the pore size can be determined from the temperature at which the condensate solidifies and the pore volume can be determined from the amount of energy involved. An important advantage of this method is that information is obtained about the internal size of the pores and not of their entrances [12,13]. The theory of thermoporometry will be summarized in section 3.1.1. A full description is given by Brun et al. [12].

We have applied thermoporometry to a series of mesoporous materials of the MCM-41 type with various pore diameters [5] for measuring their pore size and volume, surface area, wall thickness and the so-called shape factor. The results obtained are compared with nitrogen physisorption data.

2. Experimental

2.1. SYNTHESIS

MCM-41 samples 1–5 with various pore sizes were synthesized by applying dodecyl-, myristyl-, cetyl-, and octadecyltrimethylammonium bromide, respectively (purchased from Aldrich and ACROS Chimica) as the template, which is a modification based on ref. [14], except for sample 4. Cetyltrimethylammonium bromide ($C_{16}H_{33}(CH_3)_3NBr$) with addition of the auxiliary compound mesitylene (MES, 1,3,5-trimethylbenzene, ACROS Chimica) was used to prepare MCM-41 material 6 with the largest pore size studied ($MES/C_{16}H_{33}(CH_3)_3NBr = 1.0$) [5]. The synthesis formulations were heated in a polypropylene bottle at 100°C for 48 h. After cooling to room temperature, the solids were collected by filtration and washed with distilled water. The product was dried under vacuum at 90°C. The residual template was removed by calcining the samples for 10 h in air with a heating rate of 1°C/min from room temperature to 540°C.

2.2. TECHNIQUES

2.2.1. X-ray diffraction

The calcined samples were characterized by X-ray powder diffraction on a Philips PW 1840 diffractometer using monochromated Cu Kα radiation. Patterns were recorded from 1° to 10° (2θ) with a resolution of 0.02° and a count time of 10 s at each point.

2.2.2. Nitrogen physisorption measurements

Multipoint BET surface areas, pore volumes and pore size distributions of the MCM-41 materials were calculated from N_2 adsorption/desorption isotherms at −196°C using a Quantachrome Autosorb 6 instrument. The samples were outgassed for 16 h under vacuum at 350°C prior to use.

2.2.3. Thermoporometry measurements

Thermoporometry measurements were carried out on a DSC Gold apparatus of Polymer Laboratories. First, the DSC apparatus was calibrated with a sapphire and adamantane run and by melting experiments with indium, mercury and water [15]. A small amount of a dehydrated sample (15 mg) was put in a small aluminum pan. After adding a few drops of distilled water (30 mg), the pan was sealed with an aluminum lid. The DSC-probe, containing the crimped aluminum pan, was cooled from 10°C to −80°C with a rate of 1°C/min, which is slow enough to maintain equilibrium, and subsequently heated to 10°C.

2.2.4. Transmission electron microscopy

Electron microscopy was performed with a Philips CM30ST electron microscope with a field emission gun operated at 300 kV. Through-focus exit wave reconstruction [16,17] was applied to obtain more detailed information on the walls of MCM-41. In this reconstruction one combines the information of a set of images (through-focus series) recorded at various focus values to correct for the image distortion by aberrations of the electron microscope optics. The reconstructed image represents the exit wave function, which describes the electron wave at the exit plane of the specimen. To calculate the exit wave a software program developed by Coene [18] was used. The parameters required as input for the exit wave reconstruction are: the spherical aberration: 1.35 mm, the defocus step: 8.6 nm, and the starting focus, which was estimated from minimum contrast in the image. Images were recorded with a magnification of 200 000 times. The through-focus high resolution images were recorded using a Tietz software package and a 1024 × 1024 pixel Photometrix slow-scan CCD camera having a dynamic range of 12 bits. The images were binned resulting in 512 × 512 pixel images. The samples were prepared as follows. The ground MCM-41 samples were suspended in alcohol. A copper grid coated with a microgrid carbon polymer was loaded with a few droplets of this suspension.

3. Results and discussion

3.1. THERMOPOROMETRY THEORY

The relation between the triple point temperature of a condensate inside a porous material and the curvature of the solid–liquid interphase is given by

$$\Delta S_l \, dT + v_l \, d(\gamma_{ls} \, dA_{sl}/dV_l) = 0, \tag{1}$$

where ΔS_l is the solidification entropy of the condensate, T is the temperature, v_l is the specific volume of the condensate and $d(\gamma_{ls} \, dA_{sl}/dV_l)$ is the curvature of the solid–liquid interphase. Here A_{sl} is the surface of the curvature of the interphase sl and V_l the volume of the liquid, and γ is the free liquid–solid surface extension energy [12].

The most likely solidification process [12] is freezing of the condensate by nucleation inside the pores. This process can only occur if no supercooling of the condensate takes place, which is unlikely in the case of a highly divided fluid inside a porous material. The curvature of the solid–liquid interphase is in this case equal to the pore radius R_p, but molecular layers which are in contact with the pore wall will not solidify. According to Brun et al. these non-solidifying layers are for water and benzene, 2.5 molecules (8.0 Å) and 3.5 molecules (13.3 Å) thick, respectively [19–21]. It is noteworthy, that the non-freezing layers of adsorbed water agree very well with recent data obtained by NMR spectroscopy, which showed a value between 2.5 and 3.0 [22]. Therefore, more correctly, the curvature radius of the solid–liquid interphase will equal R_n, which is R_p minus the non-solidifying layer. Assuming the form of the initial nuclei to be spherical from $\Delta T = f(R_p)$ eq. (2) is obtained,

$$1/R_n = 1/2\gamma_{ls} \int_{T_0}^{T} (\Delta S_l/v_l) \, dT, \tag{2}$$

where T_0 is the triple point temperature. This equation allows for each temperature T to determine the radius of the pores. Brun et al. measured the free surface extension energy for water and benzene by measuring the freezing point depression (ΔT) of various alumina porous plugs with known texture and different pore radii. Assuming γ_{ls} to vary linearly with the temperature the resulting relation for water is

$$\gamma_{ls} = (40.9 + 0.39 \, \Delta T) \times 10^{-3}. \tag{3}$$

Substituting eq. (3) in the integrated eq. (2) leads to a relationship between the freezing temperature depression of a capillary condensate of water saturating a porous material and the pore radius R_n:

$$R_p = -64.67/\Delta T + 0.57. \tag{4}$$

The pore volume represented by pores of a particular size can be calculated from the amount of energy involved in solidification of the condensate at a specific ΔT. The signal y of the calorimeter is proportional to the amount of energy involved:

$$dV/dR_p = v_l \Delta T^2 y/(W_a mkC), \tag{5}$$

where m is the weight of the sample, k is the rate of heating, C is a constant (64.67 for water) and W_a is the apparent solidification energy of a capillary condensate. The relation between triple point temperature depression and W_a of solidification is

$$W_a = -5.56 \times 10^{-2}\,\Delta T^2 - 7.43\,\Delta T - 332 \tag{6}$$

and the melting energy is

$$W_a = -0.155\,\Delta T^2 - 11.39\,\Delta T - 332\,. \tag{7}$$

Brun et al. showed that the numerical relations for solidification for water are certainly valid in the temperature range $0 > T > -40$°C. However, the extrapolated curve for the triple point depression in porous materials shows that the relations can also be used at lower temperatures.

Thermoporometry discerns two pore shapes, namely cylindrical and spherical. In the case of spherical pores the solid–liquid interphase during solidification is the same as the interphase during melting, and the solidification temperature of the liquid inside the pores is the same as their melting temperature. Cylindrical pores show hysteresis between the solidification and the fusion thermogram. Materials with an "intermediate" pore shape can be classified by calculating a dimensionless thermodynamic shape factor f_t, which is 1.0 in the case of pure spheres and 2.0 for pure cylinders,

$$f_t = 1 - [(1 - R_{pc}/R_p)/(1 - t/R_p)]\,, \tag{8}$$

where t is the thickness of the non-solidifying layer, R_{pc} is the pore radius calculated from the melting thermogram assuming that the pores are cylindrical and R_p is the real pore radius as calculated from the solidification thermogram. This method was applied to experimental and simulated thermoporometry data of γ-alumina and nickel fluoride [12]. A good correlation was obtained between both results.

3.2. RESULTS

Powder X-ray diffraction data concerning the studied MCM-41 materials with various pore sizes are summarized in table 1. The MCM-41 materials with increasing surfactant chain length show an increase in well-defined d_{100} reflections in the X-ray diffraction patterns with some intensity at the d_{110} and d_{200} positions (fig. 1), which are characteristic for hexagonal mesopores. The all silica MCM-41 sample 5 shows clearly well-defined patterns, which can be indexed on a hexagonal lattice.

The pore size distribution, pore volume and surface area of the synthesized MCM-41 materials were measured by thermoporometry. Fig. 2 shows a typical solidification and melting thermogram of MCM-41 sample 5 with a pore size of around 40 Å going from 10 to −60°C and reverse provided by the DSC apparatus.

Table 1
Aluminosilicate MCM-41 samples

Sample	Si/Al gel	Surfactant chain length[a]	d_{100} spacing calcined (Å)	a_0[b] (Å)
1	14	12	35	40
2	14	14	36	42
3	20	16	37	43
4	∞	16	33	39
5	14	18	46	53
6	20	16 + MES[c]	56	65

[a] Number of carbon atoms in surfactant $C_nH_{2n+1}(Me)_3N^+$.
[b] Unit cell dimension, $a_0 = 2d_{100}/\sqrt{3}$.
[c] Addition of auxiliary mesitylene (MES).

The two small peaks at −45°C and −39°C reflect solidification and melting of the water inside the pores, respectively. The two large peaks represent the bulk water outside the pores. Table 2 shows data derived from thermoporometry on the six MCM-41 samples. To investigate the validity of thermoporometry a comparison was made with nitrogen physisorption data (table 3), which are in harmony with literature data [6–8]. Adsorption isotherms of nitrogen on three MCM-41 samples are shown in fig. 3. Only MCM-41 sample 6 shows an isotherm of the type IV of the IUPAC classification [2]. A reversible type IV isotherm is shown by samples 3, 4 and 5. The isotherms of the MCM-41 samples 1 and 2 seem to be both of the type I. The mesopore volumes were calculated in two ways, namely assuming it is the difference between total volume and micropore volume calculated by the De Boer t-plot [23] (denoted as volume$_{t\text{-plot}}$) or by calculating the cumulative volume in the narrow range of mesopores (denoted as volume$_{cum}$). In case of the former method it was assumed that the interparticle voids are negligibly small. All the studied MCM-41 materials showed the typical t-plot curve for mesopores with $t = 0$

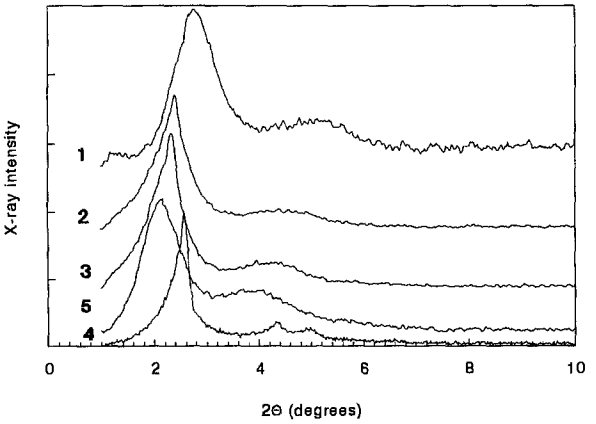

Fig. 1. Powder X-ray diffraction patterns of calcined MCM-41 samples 1–5.

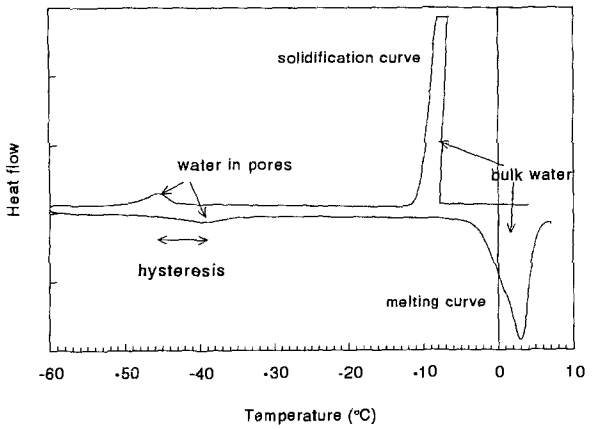

Fig. 2. Typical solidification and melting thermogram of water on MCM-41 with a pore size of about 40 Å.

intercepting the origin, which is typical for mesopores. It may be noted that the suggestion that the latter property is an indication of non-detectable micropores is a misinterpretation of the *t*-plot [10]. The micropore volume is calculated by the intercept of the back-extrapolated plateau [23].

A comparison of the two methods shows that the mesopore volumes and surface areas give a fairly good agreement, except the volume$_{t\text{-plot}}$ values which are too large. Considering mesopores it can be suggested that the De Boer *t*-plot gives too large pore volumes. Also the surface area provided by thermoporometry and the nitrogen multipoint BET area show a good correspondence, though the latter are significantly larger. The pore diameters of the MCM-41 samples provided by thermoporometry are also larger than the nitrogen pore sizes D_p. However, a very good correlation is obtained with the thermoporometry data when the corrected Kelvin equation for cylindrical pores of De Boer is applied [24].

Table 2
Thermoporometry data of the synthesized MCM-41 samples

Sample	D_p (Å)	Pore volume (cm^3/g)	Surface area [a] (m^2/g)	f_t	D_p-range (Å)
1	30	0.720	884	1.15	27–67
2	34	0.676	785	1.10	28–57
3	39	0.731	755	1.10	31–63
4	37	0.436	478	1.09	32–45
5	41	0.619	596	1.17	35–57
6	52	0.642	534	1.50	35–92
6 [b]	49	0.826	722	1.37	37–67

[a] Assuming cylindrical pores.
[b] Benzene as adsorbate.

Table 3
Nitrogen physisorption data of some MCM-41 samples

Sample	D_p[a] (Å)	D_p[b] (Å)	Volume$_{cum}$[c] (cm^3/g)	Volume$_{t\text{-plot}}$[d] (cm^3/g)	BET area (m^2/g)	D_p-range[b] (Å)
1	22	29	0.527	0.960	916	22–60
2	25	33	0.680	1.661	1016	23–63
3	27	36	0.847	2.180	1091	22–50
4	25	33	0.756	1.002	1119	22–37
5	31	41	0.800	1.885	1035	23–55
6	39	50	0.820	1.393	893	28–66

[a] Classical Kelvin equation.
[b] According to corrected Kelvin equation for cylindrical pores of De Boer [24].
[c] Cumulative volume.
[d] Calculated by the De Boer t-plot [23].

The pore size ranges of the synthesized MCM-41 products, calculated from the pore size distribution diagram where $dV/dR_p = 0$ intercepts the dR_p axis, are summarized in table 2. These pore size ranges (D_p-range) are comparable with those provided by nitrogen physisorption.

Benzene can only be used as an adsorbate when the free space inside the pores of MCM-41 (pore radius minus the non-solidifying layers) is large enough for measuring its solidification energy, which is only the case for the MCM-41 sample 6 with a size of 52 Å. Table 2 shows that thermoporometry with benzene as the adsorbate gives a slightly smaller pore diameter, but a fairly higher pore volume and surface area, which give better agreement with nitrogen physisorption. When considering the applicability of other absorbates in thermoporometry it should be noted that the adsorbate should preferably have a melting point around 0°C and a high solidification and melting energy. The lower alcohols, methanol and ethanol,

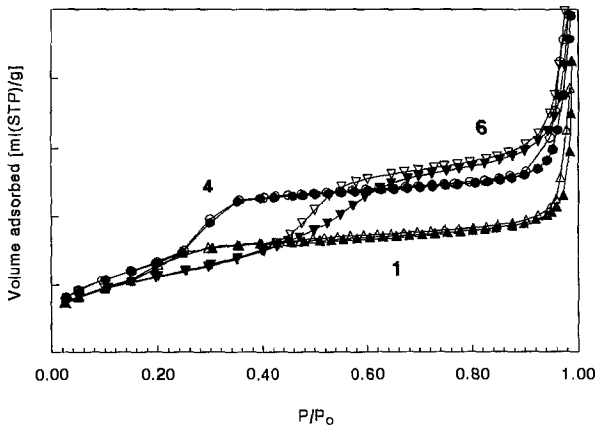

Fig. 3. Adsorption isotherms of nitrogen on MCM-41 samples 1, 4 and 6 at −196°C. Filled symbols denote adsorption and open symbols denote desorption.

are solidifying at too low temperatures, −98 and −130°C, respectively. Cyclohexane and formamide meet the requirement of a relatively high melting point.

It is generally accepted that MCM-41 possesses a hexagonal array of uniform pores with a cylindrical shape, but this was concluded from transmission electron microscopy (TEM) images and the cylindrical micelle templating mechanism [4,5]. Thermoporometry gives additional information on the pore geometry by providing the thermodynamic shape factor (f_t). Table 2 shows that the shape factors of all synthesized MCM-41 materials are between 1.09 and 1.50, which would indicate that the pores are more spherical ($f_t = 1$) than cylindrical ($f_t = 2$). Also in the case of elliptically shaped cylindrical pores a shape factor of 2 might be expected. The MCM-41 materials 1–5 show almost the same shape factor of about 1.1, which is a result of a very small hysteresis of about 3.5°C. The MCM-41 sample 6 with the largest diameter shows a larger shape factor, namely 1.5. This would suggest that the latter material is more cylindrical than the others. The deviation of the shape factor from 2 might be a result of effects like pore-blocking and/or the presence of amorphous material inside the pores (vide infra), which affect the melting curve.

TEM was performed on the samples 1, 4 and 6. Two types of morphologies were observed: (i) well ordered hexagonal and (ii) chaotic. Both morphologies are shown in fig. 4. Morphology (ii) can be explained by assuming spaghetti-like arrangements of the tubes such that a particle is like a "bowl of spaghetti" or by short tubes which are considerably shorter than the diameter of the particle; in both cases no ordering between the tubes occurs. Sample 1 contains only the chaotic morphology. Samples 4 and 6 contain a mixture of both morphologies with about 50 and 70% of ordered hexagonal material, respectively (figs. 4a and 4b).

Through-focus exit wave reconstruction was done on the hexagonal morphology of specimen 6. The resulting exit wave is shown in fig. 4b for which a series of ten images was used. Subsequent series of ten images showed a comparable result, indicating that the electron beam induced damage is rather small. The Fourier transform of the exit wave (see inset in fig. 4b) shows only the d_{10}, d_{11} and d_{20} reflections. This very limited number of reflections indicates that the projection of the walls of the tubes in the exit wave can be described with only three Fourier frequencies. This can be explained by assuming that the tube walls are not smooth but have some roughness. In projection this implies that moving from the centre of the wall to the centre of the tube the number of scattering atoms does not change suddenly from maximum to zero but shows a gradual change. In fig. 4b one can also see that some of the walls appear to be almost absent, which is probably due to a difference in approach of the surfactant–silicate aggregates during self-assembly of the mesophases [25]. There were also indications of the presence of amorphous material inside the pores. The observations of pore wall roughness and some amorphous material inside the pores applies for all the studied MCM-41 materials. The cause of the former is probably due to damage of the pore wall during calcination.

The shape factor f_t can give information on the shape of the pore by studying the degree of hysteresis. It is assumed that absence of hysteresis is due to spherically

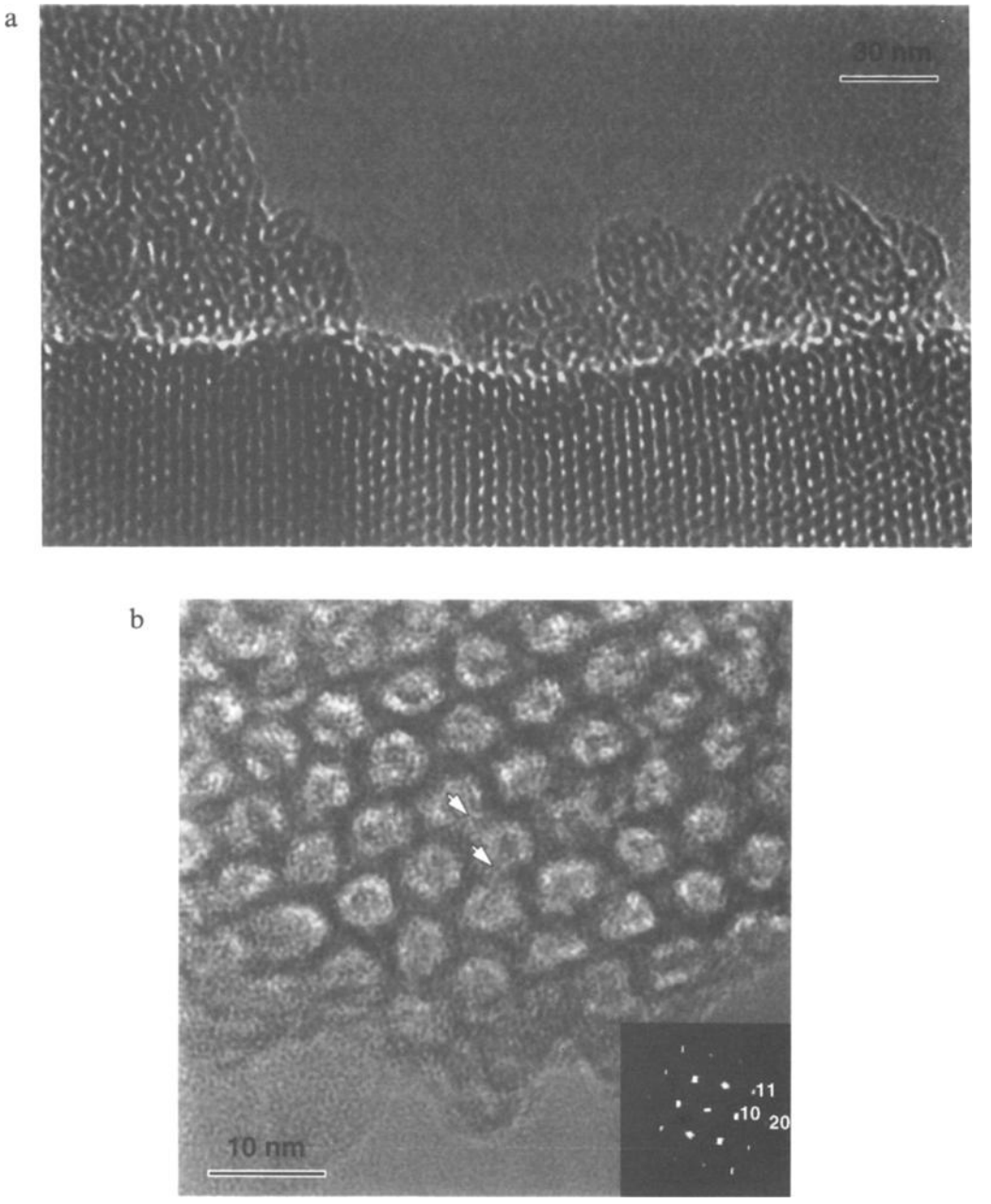

Fig. 4. (a) TEM image of sample 4 showing two morphologies of MCM-41: (i) a large hexagonal crystal and (ii) two small chaotic MCM-41 particles on top of this crystal. (b) The amplitude image of the exit wave of MCM-41 with a hexagonal structure and with a d-axis of about 60 Å. The inset shows the Fourier transform of this image with reflections up to d_{20}. Thin or partly absent walls are indicated by white arrows. The distance of the various 100 reflections is not the same, probably due to a tilt of the crystal.

shaped pores [12]. The nitrogen isotherms of the samples 1–5 show no hysteresis. However, thermoporometry on the samples 1–5 showed a hysteresis of about 3.5°C. A result of this might be the roughness of the pore wall, which causes a drastic influence on the melting process of the water inside the pores with these dimensions. It should be noted that the constant shape factor of 1.1 can not only be a result of amorphous material inside the pores, otherwise this should indicate that all these samples had the same amount of it inside the pores. Considering the difference in degree of non-crystalline material in the studied materials and the constant hysteresis effect of the samples 1–5, then it can be concluded that the shape factor is not affected by these crystallinity effects. Also other workers remarked that a decrease in the purity of the material can hardly affect the adsorption phenomena [9]. The recently reported absence of hysteresis for MCM-41 materials with a pore diameter below 40 Å [9,10] is in contrast with our results.

4. Conclusions

Thermoporometry is a promising technique for analyzing pore size distribution, pore volume and surface area of mesoporous molecular sieve materials.

The small hysteresis effect of about 3.5°C in MCM-41 materials with pore sizes below 40 Å is due to pore wall roughness effects observed by TEM. The shape factor of 1.5 deviates from the value expected for cylindrical pores, which might be caused by the presence of amorphous material inside the pores.

Acknowledgement

We are grateful to Dr. G. Hakvoort for valuable discussions and Mr. J.C. Groen for carrying out the physisorption experiments. We thank NIOK, the Dutch School of Catalysis, for financial support.

References

[1] S.J. Gregg and K.S.W. Sing, *Adsorption, Surface Area and Porosity*, 2nd Ed. (Academic Press, London, 1982).

[2] K.S.W. Sing, D.H. Everett, R.A.W. Haul, L. Moscou, R.A. Pierotti, J. Rouquérol and T. Siemieniewska, Pure Appl. Chem. 57 (1985) 603.

[3] K.S.W. Sing, Colloid Surf. 38 (1989) 113.

[4] C.T. Kresge, M.E. Leonowicz, W.J. Roth, J.C. Vartuli and J.S. Beck, Nature 359 (1992) 710.

[5] J.S. Beck, J.C. Vartuli, W.J. Roth, M.E. Leonowicz, C.T. Kresge, K.D. Schmitt, C.T.-W. Chu, D.H. Olson, E.W. Sheppard, S.B. McCullen, J.B. Higgins and J.L. Schlenker, J. Am. Chem. Soc. 114 (1992) 10834.

[6] O. Franke, G. Schulz-Ekloff, J. Rathouský, J. Stárek and A. Zukal, J. Chem. Soc. Chem. Commun. (1993) 724.

[7] P.J. Branton, P.G. Hall and K.S.W. Sing, J. Chem. Soc. Chem. Commun. (1993) 1257.
[8] P.J. Branton, P.G. Hall, K.S.W. Sing, H. Reichert, F. Schüth and K.K. Unger, J. Chem. Soc. Faraday Trans. 90 (1994) 2965.
[9] P.L. Llewllyn, Y. Grillet, F. Schüth, H. Reichert and K.K. Unger, Microporous Mater. 3 (1994) 345.
[10] R. Schmidt, M. Stöker, E.W. Hansen, D. Akporiaye and O.H. Ellestad, Microporous Mater. 3 (1995) 443.
[11] D. Akporiaye, E.W. Hansen, R. Schmidt and M. Stöker, J. Phys. Chem. 98 (1994) 1926.
[12] M. Brun, A. Lallemand, J.-F. Quinson and C. Eyraud, Thermochim. Acta 21 (1977) 59.
[13] J. Rouquérol, D. Avnir, C.W. Fairbridge, D.H. Everett, J.H. Haynes, N. Pernicone, J.D.F. Ramsay, K.S.W. Sing and K.K. Unger, Pure Appl. Chem. 66 (1994) 1739.
[14] M. Janicke, D. Kumar, G.D. Stucky and B.F. Chmelka, Stud. Surf. Sci. Catal. 84 (1994) 243.
[15] G. Hakvoort, J. Thermal Anal. 41 (1994) 1551.
[16] W.M.J. Coene, G. Janssen, M. op de Beeck and D. van Dyck, Phys. Rev. Lett. 69 (1992) 3743.
[17] H.W. Zandbergen, E.J. van Zwet, J. Jansen, J.C. Sarrao, Z. Fisk, M.B. Maple and R.J. Cava, Phil. Mag. Lett. 71 (1995) 131.
[18] W.M.J. Coene and A. Thust, Ultramicroscopy, submitted.
[19] M. Brun, A. Lallemand, J.F. Quinson and C. Eyraud, J. Chim. Phys. 6 (1973) 973.
[20] A.A. Antoniou, J. Phys. Chem. 68 (1964) 2754.
[21] G.G. Litvan, Can. J. Chem. 44 (1966) 2617.
[22] K. Overloop and L. van Gerven, J. Magn. Reson. A 101 (1993) 179.
[23] J.H. de Boer, B.C. Lippens, B.C. Linsen, J.C.P. Broekhoff, A. van den Heuvel and Th.J. Osinga, J. Colloid Interface Sci. 21 (1966) 405.
[24] J.C.P. Broekhoff and J.H. de Boer, J. Catal. 10 (1968) 377.
[25] A. Firouzi, D. Kumar, L.M. Bull, T. Besier, P. Sieger, Q. Huo, S.A. Walker, J.A. Zasadzinski, C. Glinka, J. Nicol, D. Margolese, G.D. Stucky and B.F. Chmelka, Science 267 (1995) 1138.